Transformation of hydroxyl nests in microporous aluminosilicates upon annealing

2004 J. Phys.: Condens. Matter 16 S2781

(http://iopscience.iop.org/0953-8984/16/27/013)

INSTITUTE OF PHYSICS PUBLISHING JOURNAL OF PHYSICS: CONDENSED MATTER

J. Phys.: Condens. Matter **16** (2004) S2781–S2794 PII: S0953-8984(04)73595-X

Transformation of hydroxyl nests in microporous aluminosilicates upon annealing

A A Sokol[1,4], C R A Catlow[1], J M Garcés[2] and A Kuperman[3]

[1] Davy Faraday Research Laboratory, The Royal Institution of Great Britain, 21 Albemarle Street, London W1S 4BS, UK
[2] The Dow Chemical Company, 1776 Building, Midland, MI 48674, USA
[3] Chevron Research and Technology Company, 100 Chevron Way, Richmond, CA 94802-0627, USA

E-mail: alexei@ri.ac.uk (A A Sokol)

Received 16 December 2003
Published 25 June 2004
Online at stacks.iop.org/JPhysCM/16/S2781
doi:10.1088/0953-8984/16/27/013

Abstract

Computer modelling techniques based on density functional theory are applied to modelling the structures and energies of key defect species in microporous aluminosilicates. We focus on dehydroxylation and dehydrogenation reactions of 'hydroxyl nest' defects (silicon vacancies saturated by hydroxyl groups). Our calculations chart the mechanisms and energetics of the transformation of these defects, which are introduced during the synthesis and processing of these materials.

1. Introduction

Zeolites are both natural and synthetic microporous aluminosilicate (and silica) materials, which have attracted enormous attention in recent decades owing to their applications as catalysts and sorbents, and in ion exchange. The defect structure of these materials is, however, poorly understood despite being at the heart of many of applications, particularly those in catalysis. The present paper uses simulation techniques to develop models for key defect species in this important and complex class of material.

Following the pioneering work of Barrer, Makki and Kerr [1, 2], a wide range of natural and synthetic zeolites have been shown to have remarkable thermal and chemical stability after being subjected to high temperature treatments with acids and steam—features which are of major industrial importance. In particular, Barrer and Makki reasoned: 'Hydrolysis occurs readily for the most aluminous minerals, and results in complete disintegration to colloidal silica and to aluminium salts. As the silica content increases, colloidal silica is replaced by

[4] Author to whom any correspondence should be addressed.

silica gel (9). It could be anticipated that as the silica content increases still further the gel will retain more and more 'memory' of the parent structure, so that highly specific silica-rich sorbents may be obtained.'[5] This theory was verified: the authors were able to perform the first successful dealumination procedure on a zeolitic material, Na-clinoptilolite. Furthermore, removal of aluminium from tetrahedral framework positions was postulated to occur by the intracrystalline reaction:

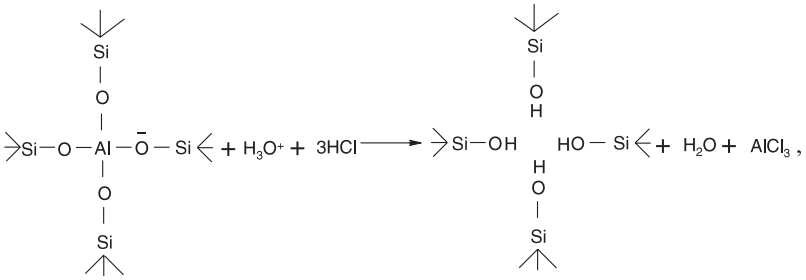

with aluminium in the framework replaced by 'hydroxyl nest' defects. Soon it was realized that acids are not crucial in the dealumination, but that steam is. In hydrogen forms of zeolites the negative charge on the framework is compensated by protons forming hydroxyl groups OH^- in the immediate vicinity of Al (Brønsted acid sites)—key defect species in these materials, which provide the Brønsted acid sites responsible for much of their catalytic activity. Kerr [2] reported an intensive water loss and dealumination in hydrogen zeolite Y upon annealing above 500 °C. He explained this observation by the reaction of constituent water at high temperatures with the framework according to:

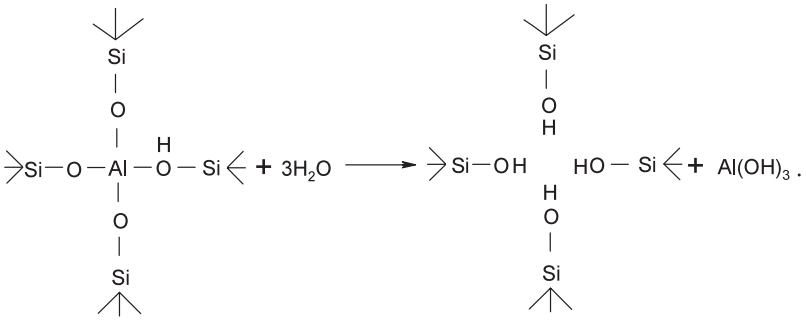

The main effect of the acid is to facilitate hydrogen exchange in non-hydrogen forms of zeolites and to dissolve aluminium debris formed by cations leaving the framework sites, which can then be washed from the zeolite pores.

Later work using various material preparation and characterization techniques demonstrated unambiguously the presence and effect of the hydroxyl nests on properties of zeolites as summarized in our recent review [3]. For clarity, we give here only a short summary of what is known about these defects. The fact that the hydroxyl nest is a cluster of four silanol groups (≡Si–OH), which are in close proximity to each other, allows their experimental identification [4–16] by

(i) a broad band 3200–3500 cm^{-1} in infrared spectra,
(ii) Q_3 and Q_2 signals in ^{29}Si chemical shift NMR spectra ascribed to tetrahedral silicon ions in the framework with one and two OH groups attached, respectively, and
(iii) a relatively narrow band 920–960 cm^{-1} observed both in infrared and Raman spectra.

[5] Referenced in [1] as (9) Murata K J 1943 *Am. Mineral.* **44** 501.

Intensive hydrogen bonding between the silanols accounts for the breadth of the OH stretching vibrational bands. The NMR silanol signal assignment is less clear as it can also be attributed to isolated terminal silanols at external surfaces of the material as well as vicinal and geminal pairs of the silanols in bulk, which is frequently referred to as the internal surface of zeolites. Finally, the assignment of the 920–960 cm^{-1} band remains ambiguous as a close signal also appears in heteroatom substituted zeolites, notably Ti-silicalite [17, 18].

Thus dealumination treatments lower the crystallinity of zeolites by producing hydroxyl nests and related defects in the zeolitic framework and filling the pores of zeolites with aluminium oxide/hydroxide debris. To clear the pores and possibly anneal the defects, further acid leaching and steaming followed by annealing (calcination) in an oxidizing atmosphere are usually applied. These treatments initiate the *healing* process, leading to the dehydration of the zeolite and the increase in its crystallinity, which is confirmed by the sharpening of the peaks in the x-ray diffraction patterns and the significant fall in intensity of the Q_3 and Q_2 signals of the ^{29}Si NMR spectra. The 3200–3500 cm^{-1} band ascribed to the stretching vibrations of the hydroxyl groups also disappears from the IR spectra. Therefore, at least partial dehydroxylation of the hydroxyl nests is seen to take place [19–22].

To rationalize this effect, three main hypotheses have been advanced [23–31]:

(i) the silicon atom in the hydroxide form migrates at elevated temperatures through the channels from the external surface, mesopores or, possibly, amorphized areas of the zeolite and refills the vacancies;
(ii) the zeolite framework reconstructs around the vacant sites forming the 'non-intact' Si–O–Si bridges between the silicon atoms from the first and second coordination shells;
(iii) hydroxyl nests aggregate and form larger pores, which, for example, is the mechanism responsible for the formation of secondary mesopore structures in mordenite and other zeolites.

The first mechanism, though plausible, cannot account for the reversibility of the healing: the hydroxyl nest defects reappear in all relevant spectra as soon as water is reintroduced into the zeolite channels. Whereas the dehydration of zeolites is a difficult process which requires long annealing at elevated temperatures, the rehydration rapidly proceeds in the ambient conditions. Moreover, the high concentration of the hydroxyl nests (up to 7% of the tetrahedral framework sites) would have been matched by the corresponding depletion of silicon from the surface or some internal regions of the zeolite which has never been confirmed by experiment. The second mechanism seems to be unlikely since the silicon atoms in the first cation coordination shell of the nest are too far from each other to allow the formation of oxide bridges. Indeed for most common zeolites, the closest silicon–silicon separation distance is 4.45 Å in sodalite, chabazite and mordenite, 4.50 Å in faujasite, 4.58 Å in ferrierite and 4.75 Å in zeolite ZSM-5. All our attempts to model the contraction of the lattice required for the bridge formation using semi-classical techniques have failed. The structures resulting from calculations have always included the breaking rather than the forming of bonds in the strained lattice around the defect site. Finally, the third mechanism is of the highest interest as the formation of secondary mesopores structures is frequently reported in the zeolite literature. However, this mechanism also fails to account for the remarkable ease with which hydroxyl nests reappear on rehydration.

To understand these processes, it is necessary to model these complex phenomena directly, in order to investigate whether the defect reconstructs into a stable low-energy immobile species or some transient mobile species is formed which can be trapped by other defects upon calcination and released in the presence of water. The internal transformation of the hydroxyl nest defect as a process that is possibly facilitated by the presence of external water, oxygen and complexation with other defects, has therefore been investigated.

First we outline our computational model and methodological approach based on previously published results for the hydroxyl nest defect. Then we consider hydroxyl nest reformation processes which conserve stoichiometry. The main focus in this paper is on two main transformation paths: (i) dehydration which requires elementary steps of deprotonation and dehydroxylation and (ii) dehydrogenation.

2. Methodological approach and model

The electronic structure calculations reported in this study were performed using density functional theory (DFT) at the PW91 level (see [32] and references therein), with periodic boundary conditions and a Γ-point approximation applied to the structure of siliceous sodalite. The cubic lattice parameter a of 8.8778 Å (cf experimental value of 8.73 Å [33]) has been obtained in our preliminary optimization of the ideal material and fixed in all subsequent calculations. A linear combination of numerical atomic orbitals as implemented in the code DMOL^3 with a double numerical basis set with polarization functions has been used throughout [34, 35]. This level of theory allowed us to obtain defect structures and formation energies in the first instance. Further work on refinement of the defect description and calculation of defect spectroscopic properties using more accurate, but necessarily more expensive treatments is underway.

The sodalite structure as the host zeolitic material has been chosen in this study as a compromise: a typical zeolite unit cell comprises of the order of 200 atoms which, due to the cost, is at the upper limit of extensive periodic DFT calculations. The unit cell of sodalite in contrast comprises only 36 atoms, which allowed us to consider a wide range of possible scenarios of the defect transformation. At the same time, this unit cell is big enough to exclude any direct overlap between defects in the adjacent unit cells as illustrated on a hydroxyl nest model in figure 1. The most stable and interesting structures we found in this study will be transferred into larger systems in our future studies.

As mentioned, we have recently reported a series of computational studies on hydroxyl nest and related defects in zeolites [3]. In particular, our calculations found two alternative conformations for this defect presented in figures 2(a) and (b). Both structures are based on a tightly bound three-membered ring of silanols. In contrast, the fourth silanol forms only weak bonds to the ring in the ground state which are readily broken in the inverted configuration at the cost of only 0.1 eV. So far only the first conformation has been reported previously based on both molecular mechanics and electronic structure, Hartree–Fock and DFT calculations on zeolites and related silica and silicate structures [36–39, 15, 16, 40]; all results are in close agreement with ours.

The transformation of the hydroxyl nest defect, as outlined above, is a complex process which includes many branches; we have been able to follow only a few. Based on our previous experience [41–43], we concentrated our investigation on the charge separation at the defect site. In a number of analogous processes, we have shown the spin polarization to be energetically less favourable whilst resulting species have already been studied in our treatment of the transformation of the Brønsted acid site to Lewis acid sites with the focus on oxygen vacancy formation. Our results for the spin polarization mechanism will be reported elsewhere.

3. Results and discussion

3.1. Nest deprotonation (proton migration)

The deprotonation of the hydroxyl nest defect represents one of the possible stages for the vacancy migration. In our model (see figure 3), the proton is transferred from the silanol

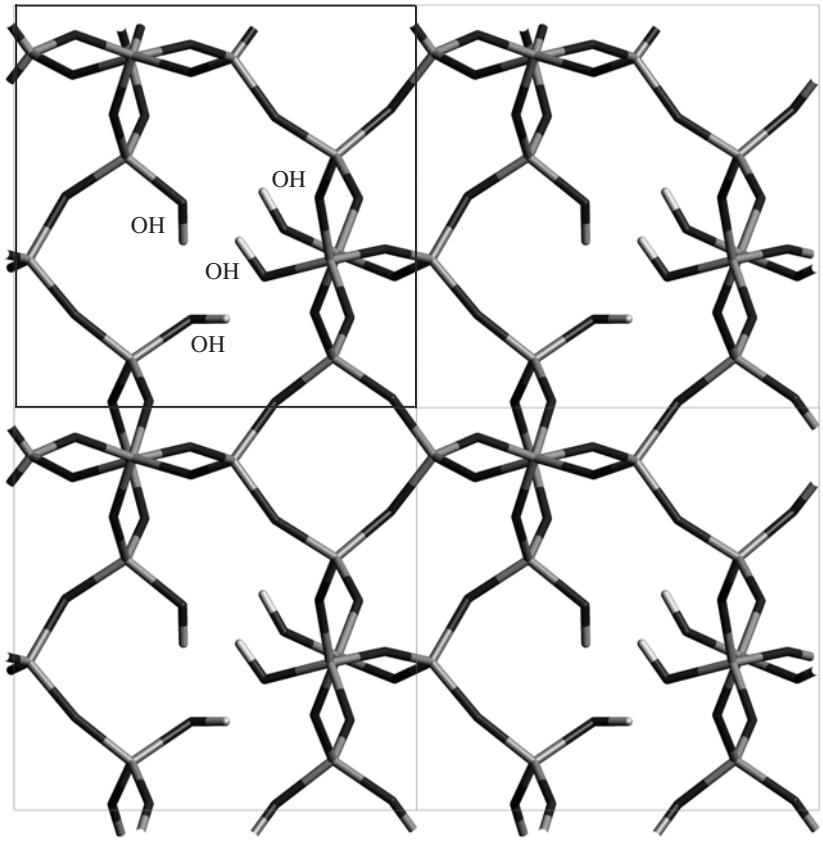

Figure 1. Hydroxyl nest defect in a periodic model based on siliceous sodalite: optimized structure. Shadings used in all figures throughout this paper: dark grey—O; medium grey—Si; light grey—H.

group, situated in the nest defect over the basal triangle, to the closest bridging oxygen. In effect, the closed ring arrangement remains intact while charge separation occurs around the deprotonated site. This results in an energy penalty of 1.8 eV, which is still one of the lowest transformation energies calculated. It can be envisaged that this process will be facilitated by such proton acceptors as water, which is in agreement with the crucial role of steam in the annealing of the hydroxyl nests and with the high temperatures (over 500 °C) at which the nest signal disappears.

Upon deprotonation, the silanol group turns into the siloxy group, a simple point defect with the formal negative charge of $-1e$, while the bridging hydroxyl group formed in the process acquires the formal charge $+1e$. Between the positively charged proton and its parent oxygen (O^-) a hydrogen bond is formed (with a bond distance of 2.3 Å), and the distance between the silicon of the siloxy group and the bridging oxygen increases to 1.8 Å. The electron localized on the O^- site is, in fact, shared by the whole siloxy group as indicated by the reduction in the effective charge on silicon and two other oxygen atoms bonded to it. The distribution of the effective charge proves that the regions of the positive and negative charge extensively overlap, so that the change in the effective charge on each group does not exceed $0.2e$ in magnitude. The deprotonation of the silanol group also strengthens its hydrogen bonding to the basal triangle.

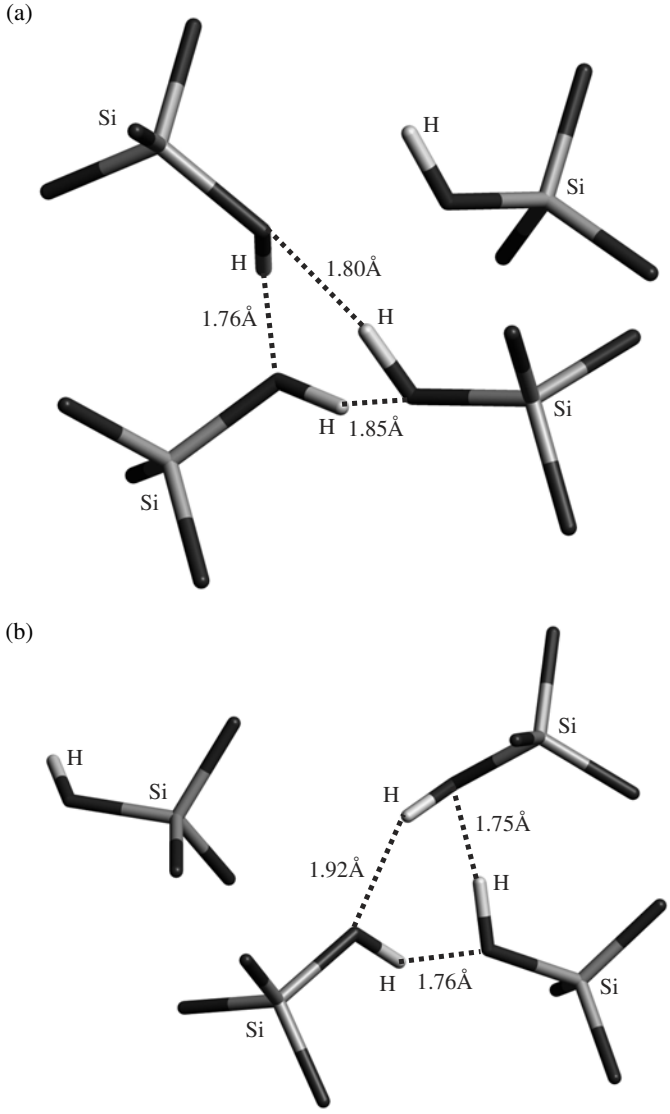

Figure 2. Hydroxyl nest. Optimized alternative structures. Three OH^- groups form a tight three-ring structure at a Si vacant site. (a) The fourth OH^- group forms two weak hydrogen bonds to the ring across the vacancy. (b) The fourth OH^- group in inverted configuration.

The double hydrogen bond formed between the siloxy species and the hydroxyl groups of the basal plane is very reminiscent of the $\equiv$Si–$O^- \cdots$ HO–Si$\equiv$ defect configuration proposed by Koller *et al* [44]. Using correlation charts, the authors have recovered the inter-oxygen separation distances of 2.70 and 2.63 Å from the ^{1}H NMR signals of 10.2 and 12.2 ppm obtained on high silica zeolites. The signals have been assigned to the hydrolysed Si–O–Si bridges with the hydrogen bonding that occurs across the defect and across the six-membered ring channel. However, as shown in [3], vicinal silanols cannot form the structure proposed by Koller *et al*. Furthermore, the formation of hydrogen bonds in that work has been confirmed by the presence of 3200 cm^{-1} band in the reported IR spectra. In our view, the model for

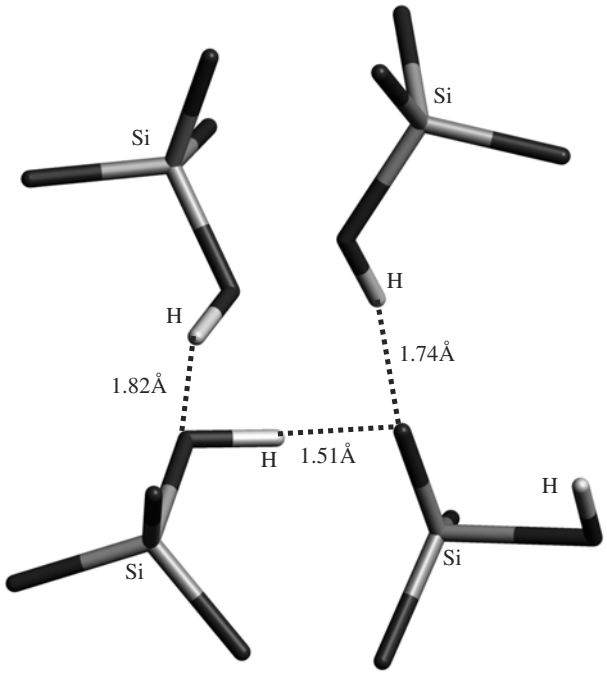

Figure 3. Model for the initial stages in proton migration from hydroxyl nest defects: optimized structure. Charge disproportionation results in the formation of strong H bonds to the Si–O^- group.

the deprotonated hydroxyl nest defect, described above, matches significantly better both the experimental data and the steric constraints on the defect structure introduced by the lattice. Indeed, we obtain the inter-oxygen separation of about 2.6 Å in the basal plane and of about 2.7 Å for the siloxy O^- ion and basal oxygen atoms.

The further deprotonation of the site due to proton hopping or facilitated by proton vehicles could lead to the protonation of the remaining two Si–O–Si bridges on the siloxy site with a consequent inversion of the silicon filling in the vacancy site and leaving a new vacancy site. Thus nest migration can be envisaged, but to establish the exact mechanism will require further investigation.

3.2. Nest dehydration

The dehydration of the nest defect is a straightforward process in which two water molecules are excluded. The process can clearly be accomplished in two steps with the removal of one water molecule in each. The nest comprises four silanol hydroxyl groups; a minimum of two should be implicated in the formation of one water molecule; one would be dehydroxylated ($-OH^-$) and another deprotonated ($-H^+$). The first step has been considered to proceed along two alternative routes. The first, requiring lower energy of about 3.8 eV, leads to the formation of the complex defect presented in figure 4.

The dehydroxylation of the silanol group situated over the basal plane, as expected, leads to the recess of the corresponding silicon into the plane of the three oxygen atoms to which it is bonded; thus the trigonal silicon, a simple defect of the formal charge $+1e$ is formed. Concomitantly, the deprotonation of one of the silanol groups in the basal plane produces a siloxy group that bears a formal charge of $-1e$, similar to the case of the deprotonated nest

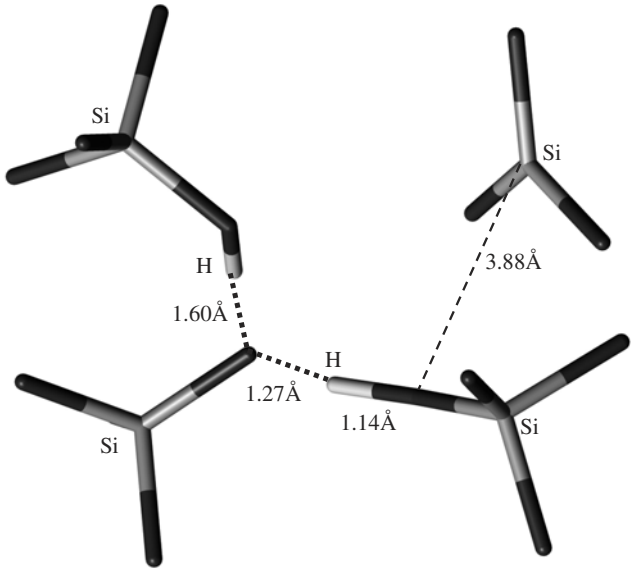

Figure 4. Model for the initial stages of hydroxyl nest defect dehydration: optimized structure. Dehydration results in the formation of a trigonal silicon site (+) and a hydrogen bridge (−) due to electron transfer. Charge is disproportionate between the two parts of the defect leading to a further strong hydrogen bond to the Si–O^- group.

considered above. However, now the deprotonated silanol group is part of the basal triangle in which the hydrogen bonds between parent silanols are much stronger. The electron previously shared by the oxygen and hydrogen, in the absence of a compensating positive charge, localizes around just one oxygen centre, which results in a much stronger Coulomb attraction for the proton of the hydrogen bonded silanol group. Geometry optimization brings the proton and oxygen together leading to the formation of the hydrogen bridge across the vacancy site.

Thus instead of the silanol coordinated to the siloxy, two siloxy groups connected through the proton $(\equiv\text{Si–O–H–O–Si}\equiv)^-$, have evolved in the relaxation process. The resulting bridge is slightly asymmetric both in its geometry and charge distribution. The charge separation in the defect region is now much more pronounced than in the case of the deprotonated nest: the charged species are separated by about 3.9 Å and the total effective charge localized in each region amounts to about $0.9e$. The top of the valence band is now defined by the electron lone pairs on the oxygen atoms that take part in the formation of the hydrogen bridge; the corresponding levels are lifted above the usually delocalized O 2p states by about 1.5 eV. The unoccupied defect states are also introduced 2.5 eV below the bottom of the conduction band, the new states being localized on the trigonal silicon site, which implies that the electron transfer would proceed between the hydrogen bridge and the trigonal silicon site upon excitation. The proton bridge structure obtained in these calculations could in fact provide an explanation for the 'delocalized proton' band in IR spectra at about 3300 cm^{-1} reported by Zholobenko *et al* [45]. The authors were able to resolve this band from a broader band with a maximum at 3500 cm^{-1}, the assignment of which was suggested to internal hydrogen bonded silanol groups in accord with the traditional interpretation. The key issue for characterization of the site would be a calculation of the O–H stretching vibrations in our future studies.

As an alternative to the mechanism for the nest dehydration, which would not require charge separation, we have considered proton transfer onto the dehydroxylated silanol site with silicon hydride formation (referred to as the 'hydride' defect). The heteropolar covalent

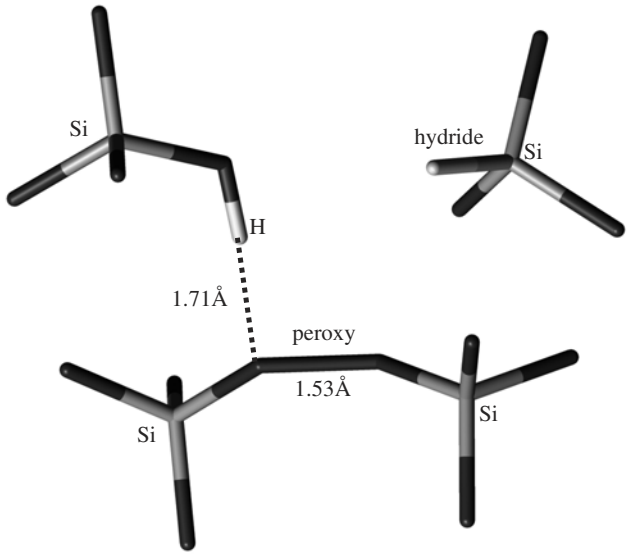

Figure 5. Model for the initial stages of hydroxyl nest defect dehydration: optimized structure. Dehydration results in the formation of a silicon hydride and a peroxy bridge due to the proton transfer.

bond formed in the hydride is able to stabilize a pair of electrons and the two remaining siloxy radical group can reconstruct to form the peroxy bridge. The resulting structure (see figure 5) is indeed a local minimum, though about 3 eV higher in energy than the hydrogen bridged nest considered above.

The hydride formation allows the dehydroxylated silicon site to retain a tetrahedral configuration. The Si–H bond length of about 1.48 Å is usual for all silicon hydride molecules where it varies between 1.47 and 1.53 Å. A similar mechanism of the silicon spin or charge 'deactivation' is often considered as a counterpart defect for the E' centre at the oxygen vacancy site in glasses. The hydride part remains well separated from the rest of the defect with the closest atom being the proton based in the silanol group (at 2.8 Å).

The formation of the peroxy bridge in the second part of the defect allows for a further electron localization on oxygen, as evident from the effective charges of -0.451 and $-0.485e$ (as compared to $-0.390e$ on each that would correspond to half of the effective charge on oxygen in the perfect siliceous material) and from the decrease in the length of the hydrogen bond formed between one of the O^- ions and the proton of the remaining silanol group. The stretching of the peroxy bridge across the vacancy site apparently introduces a stress which is also reflected in the electronic structure. The DFT band gap is now significantly narrowed to only about 2.5 eV by the states localized on the peroxy bridge so that the on-site excitations would completely define the optical adsorption, while the bonding and anti-bonding states localized on the hydride site are separated by about 8 eV lying deep in the valence and conduction bands, respectively.

The second step in the nest dehydration is unfavourable to bridge formation across the vacancy, the silicon sites being too far apart. Therefore both defect structures considered so far are further transformed into the same new defect shown in figure 6. The new defect comprises two nearly identical pairs of defects, the trigonal silicon and siloxy group arranged around the T-site vacancy. All four simple defects are at large distances (more than 3 Å each pair), which does not allow any chemical bonding effects, and interact with each other only

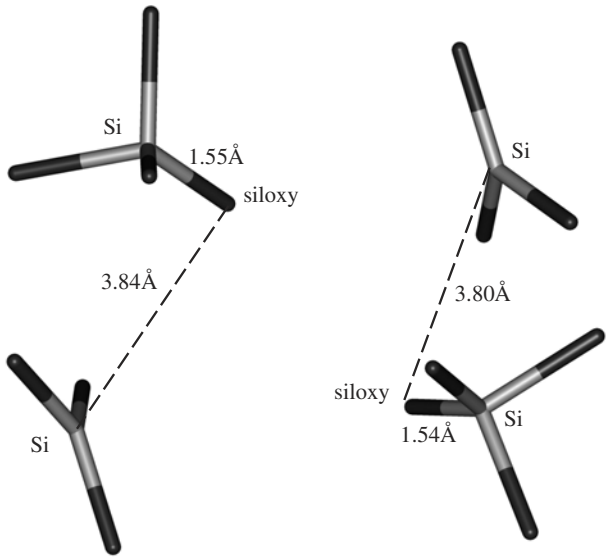

Figure 6. Model for the final stages of hydroxyl nest defect dehydration: optimized structure. Dehydration results in the formation of two pairs of trigonal silicon and siloxy species stabilized by charge disproportionation.

electrostatically. Thus chemical bonding plays an important role in defect stabilization in the first stages of the nest transformation but cannot operate in the next step which makes the complete dehydration of the defect energetically expensive (about 5.5 eV is required) and unlikely in a purely thermally activated processes. The structure of both distinct species in the defect is essentially the same as that of their precursors. The dehydroxylated silicon atoms are practically in the plane of their oxygen atoms, which reduces the corresponding Si–O bond distances down to about 1.55 Å. The excessive electron localization in the siloxy groups leads to a similar reduction in the Si–O bond distances to 1.55 Å. In both cases the decrease in the bond distances in the simple defects is accompanied by the elongation of the adjacent Si–O bonds (up to 1.70 Å), i.e. a significant atomic polarization is observed in the Si–O–Si bridges in this and other related defects which could account for the formation of the 920–960 cm^{-1} band in the IR spectra of the dealuminated zeolites. The intensive charge separation (two pairs with a charge of nearly ± 1) greatly affects the band structure. The band gap is reduced by the defect to just over 1 eV with the electrons localized in the siloxy groups (mainly on oxygen) and the first unoccupied states being due to the trigonal silicon sites.

3.3. Nest dehydrogenation

An important element in the transformation of defects in zeolites upon annealing is the presence of oxygen. Oxygen would be expected to react with hydrogen in the hydroxyl nests to form water which can be then annealed from the zeolite. However, even in the absence of oxygen, we could think of two hydrogen atoms reacting to form molecular hydrogen, which in turn can be removed from the defect site. Like the direct nest dehydration considered above, the dehydrogenation (probably facilitated by the presence of oxygen) can proceed in two steps with just one hydrogen molecule removed at a time. The energy of the first transformation has been calculated with respect to the formation of one water molecule upon reaction of the nest defect with (half of) the oxygen molecule. The two dehydrogenated sites (the $Si–O^-$) in

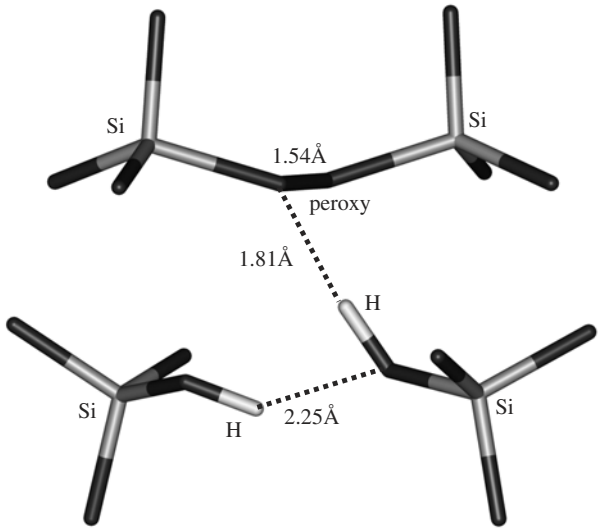

Figure 7. Model for the initial stages of hydroxyl nest defect dehydrogenation: optimized structure. Dehydrogenation results in the formation of a peroxy bridge due to the reaction of two silanols with atomic oxygen.

the singlet state of the defect have two hole spins coupled to form a peroxy bridge similar to the dehydrated nest, but with a much lower energy of about 3.2 eV. The resulting structure is shown in figure 7.

The defect includes two silanol groups which are hydrogen bonded to one another with a bond distance of about 2.3 Å and to the peroxy bridge with a shorter bond of about 1.8 Å. The structure of the simple defects only differs slightly from that already observed in the related complex defects. The effective charges on the peroxy bridge in the hydride defect are quite close: -0.485 and $-0.451e$, whereas in the current defect an electron polarization along the bridge can be observed, the effective charges being -0.531 and $-0.409e$ at the two O^- sites. However, the total charge localized on the peroxy bridge of about $0.940e$ is about the same in both cases. As with the hydride defect, the peroxy bridge introduces the defect levels into the band gap reducing its value to about 2.7 eV. The highest occupied and the lowest unoccupied levels are thus associated with the states localized on the peroxy bridge which suggests that on-site excitations should dominate the optical absorption in the current as well as in the hydride defects.

The second step of nest dehydrogenation, as expected, would require a higher energy (by about 2 eV) since no more hydrogen bonds can form to stabilize the defect. The two resulting peroxy bridges are well separated with the closest inter-oxygen distance of about 2.66 Å as shown in figure 8. Both have identical structures, the differences of about 0.01–0.02 Å arising from numerical noise in the geometry optimization procedure. The peroxy bridges are now less polarized with a difference in the effective charges of only $0.040e$ while the larger displacement of oxygen atoms (more than 1 Å) from the anionic sites of the perfect lattice leads to the lower electron localization of $-0.870e$ on each bridge.

As mentioned previously, the site can be thought of in many ways, one of which is the reconstructed silicon vacancy. This defect has been discussed in the study of the silicon self-diffusion, where the formation of Si Frenkel pairs in α-quartz and vitreous silica has been proposed to explain the migration of silicon (see [46]). The authors have argued that $Q = E_F/2 = 7.6$ eV is the formation energy in the mass action law which agrees very well

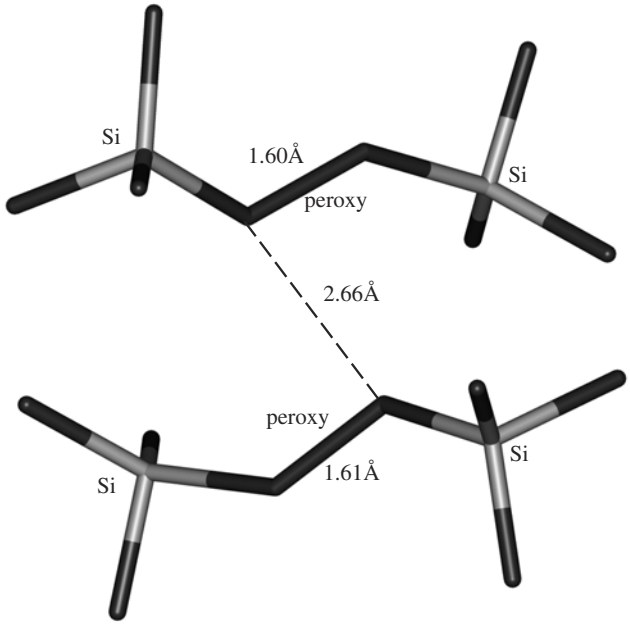

Figure 8. Model for the final stages of hydroxyl nest defect dehydrogenation: optimized structure. Dehydrogenation results in the formation of the second peroxy bridge due to a further reaction of silanols with an atomic oxygen.

with the activation energy found from the diffusion data. The Frenkel defect energy E_{F} of 15.2 eV can then be compared with our calculation for the vacancy energy of 20.7 eV. Thus the binding energy of an interstitial silicon can be estimated to be about 5.5 eV, which seems to be large for a neutral silicon. In our view, the error in this estimate lies in the use of defect formation energy instead of the barrier, which implies that the formation of the silicon vacancy proposed by Jaoul *et al* cannot be responsible for the diffusion rates measured in their experiments. Finally, the defect introduces four levels in the band gap reducing it to about 1.95 eV; the two nearly degenerate occupied states at the top of the valence band and the two nearly degenerate unoccupied states at the bottom of the conduction band being localized on the peroxy bridges. There is also a small contribution from the silicon which spans the bridges, but this is evidence of the delocalization of the defect states across the whole defect region rather than just the single ions.

4. Conclusions

The main results of this paper can be summarized in figure 9 which charts the processes for dehydration (as a concerted process of deprotonation and dehydroxylation) and dehydrogenation that follow from the calculations reported in this paper. We conclude that dehydrogenation of hydroxyl nests leading to the formation of peroxy bridges across the vacancy site is the most likely mechanism for the annealing of hydroxyl nests in the oxygen atmosphere. Deprotonation and silanol inversion that conserve the stoichiometry of the defect can also play an important role in healing the hydroxyl nests since these processes are expected to facilitate the migration and aggregation of these defects in mesopores formed in zeolitic materials upon annealing. Our calculations on related defects, following spin polarization paths for defect transformation, will be reported elsewhere shortly.

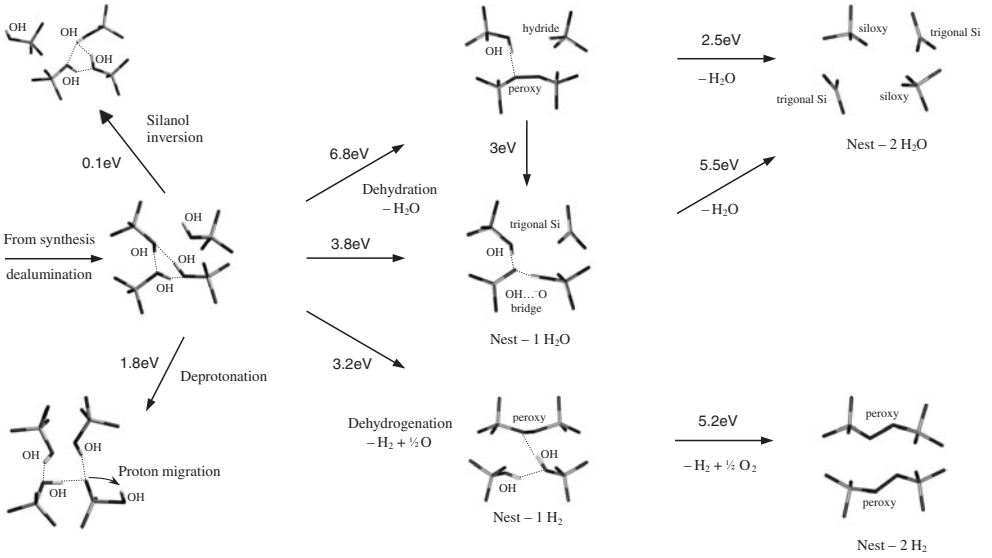

Figure 9. Models for the transformation of hydroxyl nest defects upon physico-chemical treatments. Atomic oxygen is represented by half a O_2 molecule.

Acknowledgments

We are grateful to the EPSRC for the financial support of the computational resources used in this work. AAS gratefully acknowledges financial support from the Dow Chemical Company. We are much indebted to Accelrys Inc. who provided most of the computational and visualization software used. For many useful discussions and help we would like to thank our colleagues M McAdon, J Ruiz, B Schoemann, A L Shluger, P E Sinclair, D W Lewis, S A French, S T Bromley, B Delley and D J Wilson.

References

[1] Barrer R M and Makki M B 1964 *Can. J. Chem.* **42** 1481
[2] Kerr G T 1967 *J. Phys. Chem.* **71** 4155
[3] Sokol A A, Catlow C R A, Garcés J M and Kuperman A 2002 *J. Phys. Chem.* B **106** 6163
[4] Nagy J B, Gabelica Z and Derouane E G 1982 *Chem. Lett.* **7** 1105
[5] Freude D, Frölich T, Hunger M, Pfeifer H and Scheler G 1983 *Chem. Phys. Lett.* **98** 263
[6] Sayed M, Kydd R A and Cooney R P 1984 *J. Catal.* **88** 137
[7] Fejes P, Hannus I and Kirisci I 1984 *Zeolites* **4** 73
[8] Woolery G L, Alemany L B, Dessau R M and Chester A W 1986 *Zeolites* **6** 14
[9] Dessau R M, Schmitt K D, Kerr G T, Woolery G L and Alemany L B 1987 *J. Catal.* **104** 484
[10] Dessau R M, Schmitt K D, Kerr G T, Woolery G L and Alemany L B 1988 *J. Catal.* **109** 472
[11] Kraushaar B, de Haan J W and van Hoof J H C 1988 *J. Catal.* **109** 470
[12] Yamagishi K, Namba S and Yashima T 1991 *J. Phys. Chem.* **95** 872
[13] Wu P, Komatsu T and Yashima T 1995 *J. Phys. Chem.* **99** 10923
[14] Kustov L M 1997 *Top. Catal.* **4** 131
[15] Bordiga S, Roggero I, Ugliengo P, Zecchina A, Bolis V, Artioli G, Buzzoni R, Marra G, Rivetti F, Spano G and Lamberti C 2000 *J. Chem. Soc. Dalton Trans.* **21** 3921
[16] Bordiga S, Ugliengo P, Damin A, Lamberti C, Spoto G, Zecchina A, Spano G, Buzzoni R, Dalloro L and Rivetti F 2001 *Top. Catal.* **15** 43
[17] Camblor M A, Corma A and Pérez-Pariente J 1993 *J. Chem. Soc. Chem. Commun.* 557

[18] Scarano D, Zecchina A, Bordiga S, Geobaldo F, Spoto G, Petrini G, Leofanti G, Padovan M and Tozzola G 1993 *J. Chem. Soc. Faraday Trans.* **89** 4123
[19] Beyer H K, Belenykaja I M, Mishin I W and Borbely G 1984 *Structure and Reactivity of Modified Zeolites* ed P A Jacobs *et al* (Amsterdam: Elsevier) p 133
[20] Fejes P, Hannus I, Kirisci I, Pfeifer H, Freude D and Oehme W 1985 *Zeolites* **5** 45
[21] Hunger M, Kärger J, Pfeifer H, Caro J, Zibrowius B, Bülow M and Mostowicz R 1987 *J. Chem. Soc. Faraday Trans.* I **83** 3459
[22] Kawai T and Tsutsumi K 1999 *J. Colloid Interface Sci.* **212** 310
[23] Chen N Y and Smith F A 1976 *Inorg. Chem.* **15** 295
[24] Bodart P, Nagy J B, Debras G, Gabelica Z and Jacobs P A 1986 *J. Phys. Chem.* **90** 5183
[25] Kraushaar B, van de Ven L J M, de Haan J W and van Hoof J H C 1988 *Innovation in Zeolite Materials Science* ed P J Grobert, W J Mortier, E F Vansant and G Schulz-Ekloff (Amsterdam: Elsevier) p 167
[26] van Geem P C, Scholle K F M G J and van der Velden G P M 1988 *J. Phys. Chem.* **92** 1585
[27] Fernandes L D, Bartl P E, Monteiro J L F, da Silva J G, de Menezes S C and Cardoso M J B 1994 *Zeolites* **14** 533
[28] Barras J, Klinowski J and McComb D 1994 *J. Chem. Soc. Faraday Trans.* **90** 3719
[29] Siantar D R, Millman W S and Fripiat J J 1995 *Zeolites* **15** 556
[30] Beyerlein R A, Choi-Feng C, Hall J B, Huggins B J and Ray G J 1997 *Top. Catal.* **4** 27
[31] Artioli G, Lamberti C and Marra G L 2000 *Acta Crystallogr.* B **56** 2
[32] Perdew J P and Wang Y 1992 *Phys. Rev.* B **45** 13244
[33] Richardson J W, Pluth J J Jr, Smith J V, Dytrych W J and Bibby D M 1988 *J. Phys. Chem.* **92** 243
[34] Delley B 1990 *J. Chem. Phys.* **92** 508
[35] Delley B 2000 *J. Chem. Phys.* **113** 7756
[36] Purton J, Jones R, Heggie M, Öberg S and Catlow C R A 1992 *Phys. Chem. Minerals* **18** 389
[37] Lin J S, Payne M C, Heine V and McConnel J D C 1994 *Phys. Chem. Minerals* **21** 150
[38] McConnell J D C, Lin J C and Heine V 1995 *Phys. Chem. Minerals* **22** 357
[39] Brodholt J P and Refson K 2000 *J. Geophys. Res. (Solid Earth)* B8 **105** 18977
[40] Pascale F, Ugliengo P, Civalleri B, Orlando R, D'Arco P and Dovesi R 2002 *J. Chem. Phys.* **117** 5337
[41] Catlow C R A, Sinclair P E and Sokol A A 1999 *Radiat. Eff. Defects Solids* **151** 235
[42] Catlow C R A, Corà F and Sokol A A 2000 *Comput. Mater. Sci.* **17** 312
[43] Sokol A A, Catlow C R A, Garcés J M and Kuperman A 2000 *Adv. Mater.* **12** 1801
[44] Koller H, Lobo R F, Burkett S L and Davis M E 1995 *J. Phys. Chem.* **99** 12588
[45] Zholobenko V L, Kustov L M, Borovkov V Yu and Kazansky V B 1988 *Zeolites* **8** 175
[46] Jaoul O, Béjina F, Élie F and Abel F 1995 *Phys. Rev. Lett.* **74** 2038